Role of Glutamate-268 in the Catalytic Mechanism of Nonphosphorylating Glyceraldehyde-3-phosphate Dehydrogenase from *Streptococcus mutans*†

Stéphane Marchal, Sophie Rahuel-Clermont, and Guy Branlant*

Laboratoire de Maturation des ARN et Enzymologie Moléculaire, UMR CNRS 7567, Faculté des Sciences, BP 239, Université Henri Poincaré Nancy 1, F-54506 Vandœuvre-lès-Nancy Cédex, France

Received June 21, 1999; Revised Manuscript Received December 22, 1999

ABSTRACT: Nonphosphorylating nicotinamide adenine dinucleotide (phosphate)- [NAD(P)-] dependent aldehyde dehydrogenases share a number of conserved amino acid residues, several of which are directly implicated in catalysis. In the present study, the role of Glu-268 from nonphosphorylating glyceraldehyde-3-phosphate dehydrogenase (GAPN) from *Streptococcus mutans* was investigated. Its substitution by Ala resulted in a k_{cat} decrease by 3 orders of magnitude. Pre-steady-state analysis showed that, for both the wild-type and E268A GAPNs, the rate-limiting step of the reaction is associated with deacylation. The pH dependence of the rate of acylation of wild-type GAPN is characterized by the contributions of distinct enzyme protonic species with two pK_as of 6.2 and 7.5. Substitution of Glu-268 by Ala resulted in a monosigmoidal pH dependence of the rate constant of acylation with a pK_a of 6.2, which suggested the assignment of pK_a 7.5 to Glu-268. Moreover, the E268A substitution did not significantly affect the efficiency of acylation of GAPN, showing that Glu-268 is not critically involved in the acylation, which includes Cys-302 nucleophilic activation and hydride transfer. On the contrary, the drastic decrease of the steady-state rate constant for the E268A GAPN demonstrated the essential role of Glu-268 in the deacylation. At basic pH, the solvent isotope effect of 2.3, characterized by a unique pK_a of 7.7, and the linearity of the proton inventory showed that the rate-limiting process for deacylation is associated with the hydrolysis step and suggested that the glutamate form of Glu-268 acts as a base catalyst in this process. Surprisingly, the double-sigmoidal form of the pH−steady-state rate constant profile, characterized by pK_a values of 6.1 and 7.4, revealed the high efficiency of the deacylation even at pH lower than 7.4. Therefore, we propose that the major role of Glu-268 is to promote deacylation through activation and orientation of the attacking water molecule, and in addition to act as a base catalyst at basic pH. From these results in relation to those recently described [Marchal, S., and Branlant, G. (1999) *Biochemistry 38*, 12950−12958], a scenario for the chemical catalysis of GAPN is proposed.

NAD(P)[1]-dependent aldehyde dehydrogenases (ALDH) catalyze the oxidation of a wide variety of aldehydes into acidic compounds via a two-step chemical mechanism. First, the acylation step involves the formation of a covalent thiohemiacetal intermediate, which precedes the oxidoreduction process that leads to a thioacyl intermediate and NAD(P)H. Second, the deacylation step includes the attack of a water molecule on the thioacyl intermediate, release of the acid product and of the reduced cofactor, and any potential isomerization step. The fact that most ALDHs studied so far show high catalytic efficiency implies prerequisites with respect to the chemical catalysis. First, the essential Cys should be both accessible and in the thiolate form to efficiently attack the aldehyde group at a physiological pH. Given the pK_a of a free thiolate residue, i.e., 8.9, this implies that the protein environment of the catalytic site is designed so that the essential Cys pK_a is decreased, thereby increasing the nucleophilicity of this group at a neutral pH. Second, the hydride transfer from the hemithioacetal intermediate toward the C-4 position of the nicotinamide ring of the cofactor should also be activated. Third, the nucleophilic character of the water molecule involved in the deacylation step must be strongly enhanced. Additionally, the different intermediates should be stabilized.

Several invariant residues have been shown to be critical for the chemical mechanism of ALDHs. In particular, Cys-302 has been shown to act as the essential nucleophile by site-directed mutagenesis (*1*, *2*). Substitution of Glu-268 by either Ala (for *Vibrio harveyi* ALDH) or Asp or Lys (for class 2 human ALDH) results in a decrease of the k_{cat} value for the ALDH-catalyzed reaction by at least 2 orders of magnitude without any change in the apparent K_M values

† This research was supported by the Centre National de la Recherche Scientifique and the University Henri Poincaré Nancy I.

* Corresponding author: phone +33 383 91 20 97, fax +33 383 91 20 93, e-mail guy.branlant@maem.uhp-nancy.fr.

[1] Abbreviations: ALDH, aldehyde dehydrogenase; D,L-G3P and D-G3P, D,L- and D-glyceraldehyde 3-phosphate; E268A and E268Q: Glu-268 → Ala and Glu-268 → Gln mutants of GAPN; GAPDH, phosphorylating glyceraldehyde-3-phosphate dehydrogenase; GAPN, nonphosphorylating glyceraldehyde-3-phosphate dehydrogenase; k_{ac} and k_{ss}, measured acylation and steady-state rate constants; k_{ac}^{i} and k_{ac}^{max}, intermediate and maximum pH-independent acylation rate constants; k_{ss}^{i} and k_{ss}^{max}: intermediate and maximum pH-independent steady-state rate constants; NAD(P) and NAD(P)H, nicotinamide adenine dinucleotide (phosphate), oxidized and reduced forms; pL, pH or pD; SIE, solvent isotope effect; TES, *N*-[tris(hydroxymethyl)methyl]-2-aminoethanesulfonic acid; MES, 2-(*N*-morpholino)ethanesulfonic acid; Tris, tris(hydroxymethyl)aminomethane.

10.1021/bi9914208 CCC: $19.00
Published on Web 03/04/2000

for substrates and cofactors (*3*, *4*). These mutations also suppressed the pre-steady-state burst of NAD(P)H observed on the wild-type enzymes. This result was interpreted as Glu-268 playing a role in promoting the nucleophilicity of Cys-302 rather than being only involved in the deacylation and hydride transfer steps (*3*). More recently, evidence was put forward for the chemical activation of essential Cys-302 upon cofactor binding to nonphosphorylating glyceraldehyde-3-phosphate dehydrogenase (GAPN) from *Streptococcus mutans* (*5*), a member of the ALDH family close to the class 2 mammalian enzymes. Specifically, it has been shown that cofactor binding causes a strong increase of the reactivity of Cys-302, associated with a pK_a shift from 8.5 to 6.1. Moreover, deprotonation of the side chain of an amino acid with apparent pK_a 7.6 appears to increase the reactivity of Cys-302 by a factor of 3 at a high pH.

In the present study, the kinetic properties and the rate-limiting steps of both the wild-type and E268A mutant GAPNs are described. The pH dependencies of the steady-state rate constant and of the rate of the acylation step and the solvent isotopic effect on steady-state rate constant are also reported. Interpretation of this set of results participates in the assignment of the apparent pK_a 7.6 to the Glu-268 side chain both in the binary and in the ternary complexes. We also propose that in GAPN the major role of Glu-268 is to orient and activate the water molecule involved in the deacylation. In addition, we conclude that Glu-268 has no essential role in the catalysis of the acylation step. From these results and interpretations in relation with other published kinetic data on class 2 ALDH, we propose a scenario for the chemical catalysis of GAPN.

MATERIALS AND METHODS

Materials. Wild-type and E268A mutant GAPN were produced and purified as already described (*5*). GAPN concentration was determined spectrophotometrically as the apo form by using a molar extinction coefficient of 2.04×10^5 $M^{-1}\cdot cm^{-1}$. Enzyme concentrations are expressed either as tetramer (molarity, M) or monomer (normality, N) concentration. All other materials were reagent-grade or better and were used without further purification. NAD(P) (Boehringer, Mannheim) was dissolved in H_2O and the stock concentration was determined spectrophotometrically by using a molar extinction coefficient of 18 000 $M^{-1}\cdot cm^{-1}$. D,L-G3P or D-G3P (Sigma, St. Louis, MO) was hydrolyzed from D,L-G3P diethyl acetal or from D-G3P diethyl acetal, respectively, according to the manufacturer and enzymatically titrated with GAPN.

Ionic strengths were deduced from conductance measurements on a Meterlab CDM 210 conductivity meter calibrated by NaCl solutions in the 0−0.3 M concentration range.

Steady-State Kinetic Analyses. All assays were carried out on a Kontron 933 spectrophotometer, following the appearance of NADPH at 340 nm. The reaction was performed in a 1 mL, 1 cm light path OS cuvette maintained at a temperature of 25 °C by use of a circulating water bath. Initial velocity patterns for the wild-type and mutant enzymes were obtained over the appropriate range of NADP concentrations (10−500 μM) at a series of fixed levels of D-G3P under the following conditions: 50 mM TES/NaOH buffer, pH 8.5, and 5 mM β-mercaptoethanol (ionic strength 0.05 M).

For each enzyme, the multiple data sets were analyzed by double-reciprocal plots of initial velocities v against NADP concentrations. Data were then fitted from replots of slopes from the initial plots vs reciprocal D-G3P concentration (low range [D-G3P]) or D-G3P concentration (high range [D-G3P]) and of $1/v$ axis intercepts vs reciprocal D-G3P concentration, according to the appropriate rate equation described by Segel for a general sequential mechanism with competitive substrate inhibition (*6*). In this mechanism, NADP acts as the first-binding substrate and D-G3P acts both as the second-binding substrate and as a competitive inhibitor:

$$\frac{v}{V_{max}} = \frac{[A][B]}{K_D K_{M_B}\left(1+\frac{[B]}{K_i}\right)+K_{M_A}[B]\left(1+\frac{[B]}{K_i}\right)+K_{M_B}[A]+[A][B]} \quad (1)$$

where v is the initial velocity, V_{max} is the maximum velocity, A and B represent NADP and D-G3P, respectively, K_{M_A} and K_{M_B} stand for the Michaelis constants for NADP and D-G3P, respectively, K_D is the NADP dissociation constant, and K_i is the D-G3P substrate inhibition constant. The catalytic constant per enzyme site, k_{cat}, for each species is deduced by dividing V_{max} by the enzyme normality.

pH Studies. The pH dependence of the observed steady-state rate constant k_{ss} was studied over the pH range 5−9.5 with a mixed reaction buffer consisting of 120 mM Tris, 30 mM imidazole, and 30 mM acetic acid (pH set with NaOH or HCl), adjusted with 3 M NaCl to a constant ionic strength of 0.15 M, corresponding to the optimum value for the wild-type enzyme. The data were expressed as initial rate constant k_{ss} per enzyme site. The apparent pK_a parameters governing the pH dependence of steady-state (subscript ss) and pre-steady-state (subscript ac, see below) rate constants were extracted from k vs pH profiles fitted to the following general equations:

$$k = k^{max}\frac{1}{1+10^{(pK_a-pH)}} \quad (2)$$

for one-pK_a profiles, where k^{max} represents the maximum pH-independent rate constant, and

$$k = \frac{k^i(1-10^{(pK_1-pK_2)})}{(1+10^{(pK_1-pH)})(1+10^{(pH-pK_2)})}+\frac{k^{max}}{1+10^{(pK_2-pH)}} \quad (3)$$

for two-pK_a profiles, where k^i and k^{max} represent the characteristic pH-independent rate constants for two distinct enzyme forms: one "intermediate" species characterized by a deprotonated group with pK_1 and a protonated group with pK_2 and one "maximum" with both groups deprotonated, respectively, with the assumption that the acidic form does not display any activity. In this analysis, the additive contributions of the intermediate and maximum species to the observed rate are given by the first and second terms of eq 3, respectively. In the present work an error structure of constant relative error was assumed and weighting factors were inversely proportional to k^2 (*7*).

Deuterium Isotope Effects. To determine solvent isotope effects (SIE), the tris−imidazole−acetic acid/NaCl buffer (see above) was lyophilized and redissolved in D_2O. The pD of the reconstituted D_2O buffer was checked with a common glass electrode after correction of the observed pH meter reading according to the following relation to account for the isotope effect: pD = observed pH-meter reading + 0.4 (*8*). A shift of 0.5 pH unit was observed for the same buffer composition dissolved in D_2O and H_2O. All reactant solutions were freshly prepared in D_2O. No difference in GAPN UV spectra were detected between D_2O and H_2O solutions. No change in activity was observed after incubation in D_2O buffer up to 12 h. Initial rate measurements were performed at 25 °C over a pD range of 5−9.5 under the following optimum conditions: 1 mM NADP and 0.2 mM D-G3P. Control experiments were repeated in the same conditions, all reactants and buffer being reconstituted in H_2O. The similarity of the apparent pK_a shifts of the pL−k_{ss} profile (L = H or D) in D_2O vs H_2O (i.e., 0.5 pH unit) and of the pL shift for the same buffer composition ensured that equivalent pL conditions were met for GAPN. The SIE on k_{ss}, $k_{ss}^{H_2O}/k_{ss}^{D_2O}$, was plotted as a function of the pH value. The apparent pK_a parameter that governs the pH dependence of $k_{ss}^{H_2O}/k_{ss}^{D_2O}$ was then deduced from fitting experimental data to:

$$\frac{k_{ss}^{H_2O}}{k_{ss}^{D_2O}} = \frac{\left(\frac{k_{ss}^{H_2O}}{k_{ss}^{D_2O}}\right)^{max}}{1 + 10^{(pH-pK_a)}} \quad (4)$$

where $(k_{ss}^{H_2O}/k_{ss}^{D_2O})^{max}$ is the maximum observed SIE.

Proton inventories were performed at 25 °C and pD = 8.5 for the wild-type and E268A mutant GAPN, by measuring the isotope effect in D_2O/H_2O mixtures. With the assumption that the fractionation factors of protons in the ground state were close to 1, plots of the measured kinetic SIE $k_{ss}^{x}/k_{ss}^{D_2O}$ vs D_2O mole fraction (x) were fitted according to the simplified Gross−Butler equation (*9*):

$$\frac{k_{ss}^{x}}{k_{ss}^{D_2O}} = \frac{k_{ss}^{H_2O}}{k_{ss}^{D_2O}}(1 - x + \phi_T^1 x) \times ... \times (1 - x + \phi_T^n x) \quad (5)$$

thereby allowing the extraction of the number (n) of protons participating in the observed process with fractionation factors of ϕ_T^n in the transition state.

Pre-Steady-State Kinetic Measurements. Pre-steady-state kinetic analyses of wild-type and mutant GAPN were carried out on a SFM 3 Biologic Instruments stopped-flow apparatus (Biologic, Grenoble, France) with a tungsten lamp and slit of 5 nm as light source, equipped with a 1 cm light path TC 100-10 observation cuvette. As for steady-state kinetics, time courses for the reaction of each enzyme with D-G3P and NADP were followed by the appearance of NADPH monitored at 340 nm, at a constant temperature of 10 °C, over the pH range of 5−9.5. The pH was set by a series of low ionic strength (0.08 M, adjusted with NaCl) single buffers over the low-pH range (50 mM MES/NaOH buffer, 5.0 < pH < 6.5), intermediate-pH range (50 mM TES/NaOH buffer, 6.7 < pH < 8.0), and high-pH range (50 mM Tris-HCl buffer, 8.2 < pH < 9.5) (see Results). The experiment was set up with one syringe filled with wild-type or E268A enzyme (16 μN final concentration after mixing) and the other one containing NADP (saturating concentration of 1 mM after mixing) and a range of D-G3P concentrations. The continuously measured absorbance was digitized and directly analyzed as the sum of exponential and linear components with the biokine program employing nonlinear regression analysis. Analyses were carried out with the minimum number of phases necessary to fit the experimental time courses without systematic deviation. An average of five runs was recorded to perform kinetic analysis at each pH. The pH dependencies of exponential rate constants were analyzed as described in steady-state methods for k_{ss} vs pH profiles.

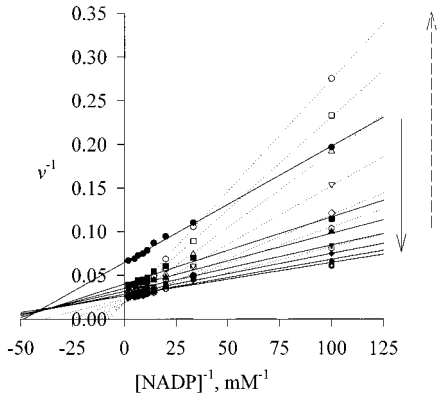

FIGURE 1: Initial velocity patterns for the wild-type GAPN-catalyzed reaction. The appearance of NADPH was followed at 340 nm under steady-state conditions at 25 °C and pH 8.5 in 50 mM TES buffer and 5 mM β-mercaptoethanol. Enzyme concentration was 12 nN. Double-reciprocal plots of initial rates vs NADP concentrations (symbols) and best linear fits (lines) were obtained over a low [D-G3P] range (solid symbols and lines), (●) 20 μM, (■) 40 μM, (▲) 60 μM, (▼) 80 μM, (◆) 100 μM, (⬢) 120 μM, and (solid hexagon with open plus) 140 μM; and over a high [D-G3P] range (open symbols, dotted lines), (open hexagon with solid plus) 160 μM, (⬡) 180 μM, (◇) 200 μM, (▽) 400 μM, (△) 600 μM, (□) 800 μM, and (○) 1 mM. The solid arrow shows the decreasing behavior of linear regression slopes vs low [D-G3P]. Note the solid lines intersecting at the left of the $1/v$ axis. The dotted arrow shows the increasing behavior of linear regression slopes vs high [D-G3P]. Note the dotted lines intersecting on the $1/v$ axis.

RESULTS

Kinetic Mechanism of GAPN under Steady-State Conditions. Since NADP and G3P are both substrates of GAPN and an inhibitory effect had been observed at high G3P concentrations, determination of true kinetic constants and of optimum conditions for the GAPN-catalyzed reaction required full analysis of the kinetic mechanism. Therefore, the steady-state bisubstrate mechanism of wild-type and mutant GAPNs was studied at pH 8.5 and temperature 25 °C according to the method of Segel (*6*). As a preliminary, enzyme activity measurements with either D,L-G3P or D-G3P showed that both enantiomeric forms behaved as equally efficient substrates for wild-type GAPN. The natural form, D-G3P, was used in subsequent mechanistic studies.

A representative data set for wild-type GAPN is presented in Figure 1 as double-reciprocal plots of initial rates vs NADP concentration. According to Segel (*6*), linearity of the plots at each D-G3P concentration, the reverse dependence of the slopes on D-G3P concentration in the low range (0.04−0.20 mM, solid lines), and convergence of the lines

Table 1: Kinetic Parameters of the Wild-Type and E268A GAPN-Catalyzed Reactions

		NADP		D-G3P	
	k_{cat} (s^{-1})	K_M (μM)	K_D (μM)	K_M (μM)	K_i (μM)
GAPN wt	60 ± 1	25 ± 2	2.1 ± 0.1	46 ± 1	540 ± 20
E268A mutant	0.06 ± 0.01	25 ± 2	2.4 ± 0.1	51 ± 1	540 ± 20

[a] Kinetic parameters were deduced from nonlinear regression of experimental data sets equivalent to Figure 1, according to eq 1 (see Materials and Methods). The steady-state initial rates of the reaction of 12 nN wild-type and 3 μN E268A GAPNs were measured at 25 °C in 50 mM TES buffer, pH 8.5, and 5 mM β-mercaptoethanol at a low ionic strength of 0.08 M.

through a common point to the left of the $1/v$ axis are consistent with an ordered sequential or rapid equilibrium random mechanism. As the fixed D-G3P concentration increases to the higher range (0.3−1.2 mM), the family of reciprocal plots remains linear (dotted lines), although they intersect on the $1/v$ axis, with slopes increasing with the substrate concentration. These data rather support an ordered sequential mechanism, with NADP acting as the first-binding substrate and D-G3P as the second-binding substrate, and D-G3P behaving as a competitive substrate inhibitor. Such a conclusion was further supported by previous experiments, which used protein fluorescence quenching to probe the conformational change leading to the catalytically competent form of GAPN (*5*). They showed that GAPN was able to bind NADP with high affinity in the absence of D-G3P. In addition, one can also take advantage of the esterase activity of GAPN: only NADP activated the acylation rate of the ester substrate *p*-nitrophenylacetate on apo-GAPN, while D-G3P did not significantly affect this rate (data not shown), which constitutes another piece of data in support of the ordered mechanism with NADP binding first.

Table 1 summarizes the kinetic parameters deduced from the analysis of such data sets according to eq 1 for the wild-type and E268A mutant enzymes. This method not only allows the determination of K_M values for NADP and D-G3P, 25 μM and 46 μM, respectively, for wild-type GAPN, but also of the NADP dissociation constant, 2.1 μM, and of the D-G3P inhibition constant, 540 μM, for wild-type GAPN. Very similar values were obtained for the mutant. Optimum activity conditions were observed at 1 mM NADP and 0.2 mM D-G3P.

While the substitution of Glu-268 by Ala has nearly no effect on the substrate and cofactor parameters, this mutation strongly affects the rate of the GAPN-catalyzed reaction. At pH 8.5, 25 °C, and ionic strength of 0.08 M, the E268A mutation results in a 1000-fold decrease of the catalytic constant k_{cat} from 60 to 0.06 s^{-1}.

Evidence That the Rate-Limiting Step of the Wild-Type and Mutant GAPN-Catalyzed Reaction is Associated with Deacylation. Following the appearance of NADPH at 340 nm under pre-steady-state conditions by fast kinetic methods allows one to easily identify the major rate-limiting segment of the reaction: if the rate of NADPH production, which is associated with the acylation, is faster than the subsequent deacylation phase, then a burst of reduced cofactor production could be monitored kinetically. Consequently, the rate-limiting process can be associated with deacylation.

Preliminary experiments conducted at pH 6.0, 25 °C, and ionic strength of 0.15 M already suggested such behavior for both enzyme species. For the wild-type enzyme at a basic pH, however, both phases appeared to be too fast to be clearly resolved. To achieve adequate resolution for kinetic analyses through the full pH range (5.0−9.5), the temperature and ionic strength conditions were lowered to 10 °C and 0.08 M, respectively. This combination resulted in a sufficient decrease of the rate of both phases to allow observation and kinetic resolution. For example, at basic pH, wild-type GAPN showed a fast process with rate constant of 210 s^{-1}, followed by a 10-fold slower phase of 22 s^{-1} (Table 2). Under these conditions at all pH values tested, the pre-steady-state kinetics of the reaction catalyzed by wild-type and E268A mutant GAPN consisted of a single-exponential burst of NADPH production, the amplitude of which corresponds to 4 mol/mol of tetrameric enzyme, followed by a slower linear phase. These observations supported that the global deacylation step was rate-limiting for the catalyzed reaction at 10 °C and 0.08 M ionic strength.

pH Dependence of the Acylation Step Rate Constant. Due to D-G3P competitive inhibition, optimal activity conditions (0.2 mM D-G3P) do not correspond to strictly saturating concentrations. In these conditions, the k_{ac} vs pH curve could thus include a k_{ac}/K_M contribution. Furthermore, the apparent K_M for D-G3P in the steady-state and pre-steady-state experiments might differ from each other. Therefore, the dependence of the pre-steady-state rate constant on D-G3P concentrations (0.075, 0.1, 0.2, and 0.4 mM) was measured over the pH range of 5.0−9.0. Indeed, double-reciprocal velocity plots yield an apparent K_M value of ca. 500 μM, distinct from the steady-state value, although independent of the pH within experimental error. A strong substrate inhibition is observed for [D-G3P] > 0.2 mM.

As far as pK_a titration is concerned, although differing in amplitude, all pH−k_{ac} profiles are similar within experimental

Table 2: Parameters for the pH Dependencies of GAPN Pre-Steady-State[a] and Steady-State Kinetics[b]

	acylation[a]				steady state[b]			
	pK_1	pK_2	k_{ac}^{i} (s^{-1})	k_{ac}^{max} (s^{-1})	pK_1	pK_2	k_{ss}^{i} (s^{-1})	k_{ss}^{max} (s^{-1})
wild-type GAPN	6.2 ± 0.1	7.5 ± 0.1	52 ± 7	210 ± 5				22 ±2[c]
					6.1 ± 0.1	7.4 ± 0.2	23 ± 3	68 ± 3
E268A mutant	6.2 ± 0.1			49 ± 1	ND[d]	ND	ND	ND

[a] pK_a and k_{ac}^{max} values were deduced from nonlinear regression of Figure 2 experimental data collected at 10 °C, 0.08 M ionic strength, and 0.2 mM D-G3P, according to eq 2 or 3 (see Materials and Methods). Other experimental details are given in the legend of Figure 2. [b] pK_a and k_{ss}^{max} values were deduced from nonlinear regression of Figure 3 experimental data collected at 25 °C and ionic strength of 0.15 M according to eq 2 or 3 (see Materials and Methods). Other experimental details are given in the legend of Figure 3. At least two independent determinations were performed to determine each constant. [c] Steady-state rate constant of the wild-type reaction measured at 10 °C and ionic strength 0.15 M. [d] ND, not determined.

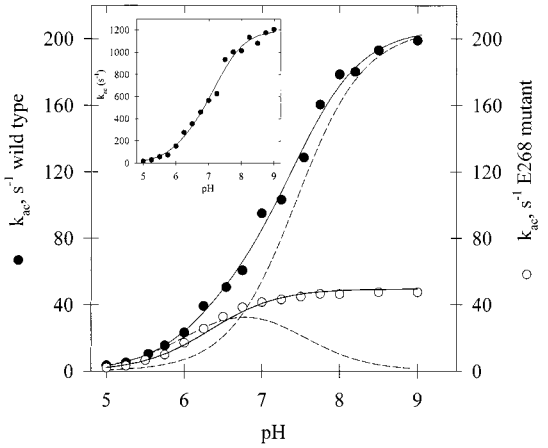

FIGURE 2: Representative pH dependence of the acylation rate constant k_{ac} for the GAPN-catalyzed reaction. Pre-steady-state exponential burst of NADPH production was followed at 340 nm at 10 °C on a stopped-flow apparatus, by rapidly mixing 16 μN enzyme, 1 mM NADP, and 0.2 mM D-G3P (final concentrations). pH was set by a series of buffers at a constant ionic strength of 0.08 M. Wild-type experimental data (●) were analyzed by nonlinear regression against eq 3, identified by a best fit theoretical curve (solid line). The contribution of each of the protonic states to k_{ac}, provided by the individual terms of eq 3, is represented by the dashed curves. The inset shows the corresponding profile obtained by extrapolation of the rate at saturating D-G3P concentration at each pH value. E268A experimental data (○) were analyzed by nonlinear regression against eq 2, identified by best-fit theoretical curves (solid line).

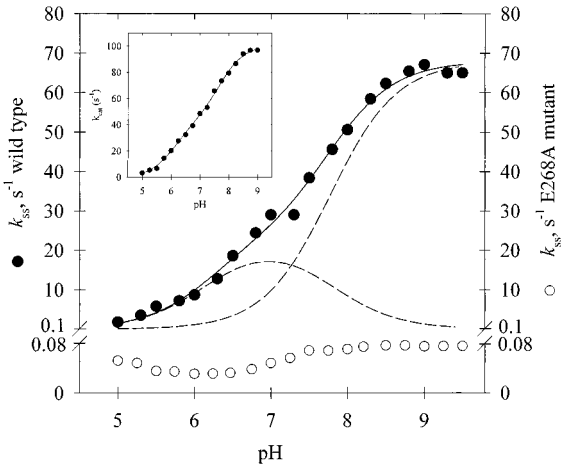

FIGURE 3: Representative pH dependence of the steady-state rate constant for wild-type and E268A GAPN-catalyzed reactions. The oxidation of 0.2 mM D-G3P in the presence of 1 mM NADP was monitored by the appearance of NADPH at 340 nm at 25 °C. The pH was set by a series of mixed buffers, 120 mM Tris-HCl, 30 mM imidazole, and 30 mM acetic acid at constant ionic strength of 0.15 M. Experimental data for the wild type (●) were analyzed by nonlinear regression according to eq 3, identified by best-fit theoretical curves (solid line). The contribution of each individual active protonic species, provided by the individual terms of eq 3, is represented by the dashed curves. The inset shows the corresponding profile obtained by extrapolation of the rate at saturating D-G3P concentration at each pH value. Open circles (○) represent experimental data for the E268A mutant, for which no fitting was possible (see text).

error, including the one resulting from the extrapolation of the rates at saturating D-G3P concentration. Therefore, the curve obtained at 0.2 mM D-G3P was kept as a representative of the experiment. Figure 2 and its inset show the pH dependence of the burst rate constant k_{ac} at 0.2 mM D-G3P and of the extrapolated rate constant at saturating D-G3P concentration for wild-type GAPN, respectively. Both curves exhibit an increasing double-sigmoidal profile that is adequately described by the contribution of two ionizable groups, one of apparent pK_a 6.2 ± 0.1 that must be deprotonated for acylation and one of apparent pK_a 7.5 ± 0.1 whose deprotonation activates acylation by 4-fold (summarized in Table 2). Consequently, aside from a nonreactive acidic form, two species must be considered to participate in the acylation step, an intermediate form with characteristic acylation rate constant k_{ac}^{i} of 52 s^{-1} and a basic form with optimum acylation rate constant k_{ac}^{max} of 210 s^{-1} at 0.2 mM D-G3P (see decomposition of the curve in Figure 2 and Table 2). In contrast, as apparent in Figure 2, analysis of the corresponding profiles for the E268A mutant enzyme reveals that only the deprotonation of one group with an apparent pK_a of 6.2 ± 0.1 is required to accurately fit the experimental data. In this case, the reactive basic species acylates with a rate constant value of 49 s^{-1} (Table 2).

pH Dependence of the Steady-State Rate Constant. As for the pre-steady-state experiments, to circumvent possible misinterpretations due to D-G3P competitive inhibition, the dependence of the steady-state rate constant on D-G3P concentrations (4.5, 20, 45, 100, and 200 μM) was measured over the pH range of 5.0−9.5. No change in the apparent K_M value (65 μM) was observed as a function of pH. Again, as far as pK_a titration is concerned, although differing in amplitude, all pH−k_{ss} profiles are similar within experimental error, including the one resulting from the extrapolation of the rates at saturating D-G3P concentration. Therefore, the curve obtained at 0.2 mM D-G3P was kept as a representative of the experiment. For wild-type GAPN, the overall pH−k_{ss} profile obtained at 0.2 mM and extrapolated to saturating [D-G3P] (Figure 3 and inset, respectively) appear very similar to the k_{ac} vs pH curve (Figure 2). This similarity is confirmed by the analysis of the experimental data according to eq 3, which provides similar apparent pK_a values of 6.1 ± 0.1 for a group that must be deprotonated for activity and pK_a 7.4 ± 0.2 for a group whose deprotonation leads to the replacement of a species with characteristic k_{ss}^{i} of 23 s^{-1} by a basic species characterized by a k_{ss}^{max} of 68 s^{-1} at 0.2 mM D-G3P (see decomposition of the curve Figure 3). Differences in buffer composition and ionic strength (0.15 M vs 0.08 M) explain the shift between k_{ss}^{max} (68 s^{-1}) and k_{cat} (60 s^{-1}) values. Much lower relative variations were obtained for the E268A mutant, for which the k_{ss} constant fluctuates between 0.03 s^{-1} at pH 6.2 and 0.08 s^{-1} at basic pH (Figure 3). Given the magnitude of the k_{ss} changes for this mutant, no pK_a parameters could be determined precisely.

Solvent Deuterium Isotope Effects. Several individual processes could be considered to be associated with deacylation, which has been assigned as the rate-limiting step of the GAPN-catalyzed reaction: hydrolysis of the thioacyl intermediate, possibly including the formation and the breakdown of the tetrahedral intermediate, release of the product, release of the reduced cofactor, and any potential isomerization step. To establish whether the rate-limiting step was associated with a proton-transfer process, we studied the SIE of D_2O on the steady-state rate constant of the GAPN-catalyzed reaction as a function of pH (Figure 4). Substituting D_2O for H_2O results in a (2.3 ± 0.1)-fold decrease in wild-type GAPN k_{ss} rate constant measured at a

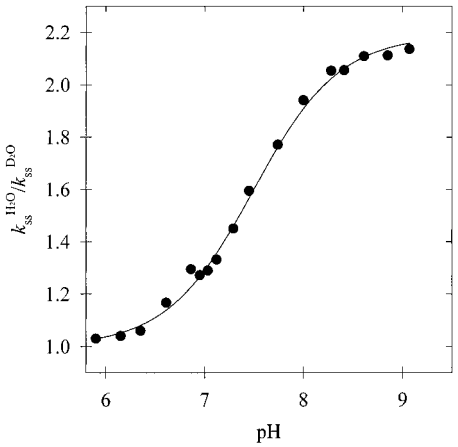

FIGURE 4: pH dependence of the solvent kinetic isotope effect on the steady-state rate constant. Experiments were conducted under conditions as in Figure 3, after reconstitution of the lyophilized buffer either in D_2O or in H_2O, in conditions of equivalent pL (see text). Apparent pK_a value of 7.7 ± 0.1 and pH-independent maximum isotope effect at basic pH of 2.3 ± 0.1 were deduced from the best fit against eq 4 (solid line).

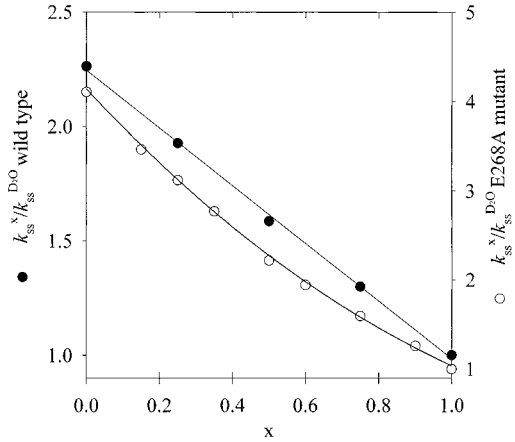

FIGURE 5: Proton inventories for deacylation of GAPN-catalyzed reaction at pH 8.5. Wild-type (●) and E268A mutant (○) experimental data were analyzed from nonlinear regression of initial velocity data to eq 5. Standard error on each experimental point was less than 2%. The solid lines represent the best-fit theoretical curves. x is the D_2O mole fraction.

basic pH (at 0.2 mM D-G3P and 1 mM NADP), which decreases to 1.1 at an acidic pH in a sigmoidal manner. Analysis of these data according to eq 4 reveals the involvement of a single ionization of pK_a 7.7 ± 0.1.

To establish how many protons contribute to the SIE on k_{ss}, proton inventory was performed at pL = 8.5 for the wild-type and E268A mutant GAPNs. For wild-type GAPN, an apparently linear dependence on D_2O mole fraction (x) was observed with k_{ss}^{x} decreasing with increasing mole fraction of D_2O. The best fit of the data against eq 5 was obtained for $n = 1$ and confirmed the apparent linearity of the plot (Figure 5).

For the E268A mutant, kinetic SIE could not be followed over the full pH range due to less accurate, very slow steady-state rate constants at acidic pH values (Figure 3). At optimum pL = 8.5, however, the SIE was 4.10 ± 0.05 and the proton inventory experiment revealed a nonlinear dependence of the isotope effect on D_2O mole fraction. Nonlinear regression analysis against eq 5 did not allow distinction between two- or three-proton mechanisms. If two protons were considered to be transferred in the rate-limiting process, the best fit was obtained for equivalent protons with ϕ_T of 0.5. For $n = 3$, fitting our experimental data could not lead to a definitive distinction between equivalent or non-equivalent protons.

DISCUSSION

Investigation of the chemical mechanism of aldehyde dehydrogenases relies on the possibility of resolving at least both main steps of the reaction, the acylation and the deacylation. In that regard, the GAPN enzyme appears as a fine mechanistic model: we show that, for both the wild-type and the mutant enzymes studied, conditions can be found such that acylation and deacylation are kinetically resolved, and that under all steady-state conditions, the deacylation is the rate-limiting step for the whole reaction. This allowed us to study the effect of pH and of active-site residue Glu-268 substitution on both phases of the reaction, including solvent isotope effect on the deacylation step.

GAPN Glu-268 Is Not Critically Involved in Acylation. Study of the rate of acylation k_{ac} as a function of pH is used to reveal ionizations that control the rate-limiting step leading to the formation of NADPH. As illustrated by the curve decomposition in Figure 2, two wild-type enzyme species acylate efficiently from pH 5 to 9, with two apparent pK_a values of 6.2 and 7.5. These pK_a could correspond to ionizations of enzyme residues, of D-G3P thiohemiacetal intermediate groups (C-1 hydroxyl or phosphate), or of the NADP within the ternary complex. Substitution of Glu-268 by Ala results in simplification of the pH−k_{ac} curve to a monosigmoidal profile characterized by a pK_a of 6.2 (Figure 2). This supports the assignment of the 7.6 pK_a to the Glu-268 side chain, as already postulated (*5*). However, other hypotheses could be raised regarding the assignment of the 7.6 pK_a. It could represent the ionization of the Glu-268 via the relay of the side chain of another amino acid with no detectable pK_a. It could also correspond to the pK_a of the side chain of another amino acid whose pK_a would be controlled by Glu-268. However, the recent determination of a crystal structure of GAPN that mimicked a transition state (Cobessi et al., submitted for publication) supports the assignment of the 7.5 pK_a to Glu-268. Most importantly, the high efficiency of acylation of E268A mutant GAPN, which is not rate-limiting over the full pH range, demonstrates that, in GAPN, Glu-268 is not critically involved in the catalysis of the acylation step. In fact, deprotonation of the Glu-268 side chain yields a new protonic species with an acylation rate increased by only 4-fold, compared to the already efficient intermediate species (k_{ac}^{max} of 210 s^1 vs k_{ac}^{i} of 52 s^{-1}).

Regarding assignment of the 6.2 pK_a, Marchal and Branlant (*5*) recently reported very similar behavior for the pH dependence of the rate of alkylation of holo-GAPN by iodoacetamide, which is based on activity measurements and only reflects the rate of alkylation of essential Cys-302. Since only the thiolate form of Cys-302 is reactive toward iodoacetamide, the alkylation method allows direct determination of the Cys-302 pK_a. In addition, no reactivity is observed at pH lower than 5.5, indicating that no thiolate species exists in this pH range. Thus, this experiment showed the titration of Cys-302 with pK_a 6.2, and of a residue with pK_a 7.6, whose deprotonation resulted in a 3-fold increase of the rate of alkylation. From the comparison of the

alkylation and acylation curves, it is tempting to assign the ionization of the 6.2 pK_a observed in the acylation to Cys-302. However, as listed above, other hypotheses can be proposed. Regarding ionizations of the 2′-phosphate group of NADP, binding into a site including Thr-195 and Lys-199 (*10*) probably shifts this pK_a from 6.1 in solution (*11*) to a lower value close to the acid limit of the pH range, such that it is not observable, this group being bound primarily as the dianion (*12*, *13*). Similar arguments are also relevant for the phosphate group of the substrate, which was postulated to bind in an anionic site comprising Arg-124 and Arg-301 (*10*). Furthermore, since the rate-determining step within acylation has been associated with hydride transfer from the isotopic effect of deuterated D-G3P (data not shown), the pK_a of 6.2 might be associated with the ionization of a group of the thiohemiacetal ternary complex, namely, the C-1 hydroxyl group. In such an hypothesis, the positive effect of Glu-268 deprotonation on the measured rate of acylation would originate from the activation of the hydride transfer process. This interpretation is in agreement with data suggesting the presence of an oxyanion site in GAPN (see last section of the Discussion).

Role of Glu-268 in Deacylation. To begin with, the drastic decrease of k_{ss} over the pH range tested for the reaction catalyzed by the E268A mutant demonstrated the essential role of Glu-268 in the deacylation step. To get further insight into the catalytic role of Glu-268, we analyzed the solvent isotope effect of D_2O on k_{ss} as a function of pH for the wild-type enzyme. The SIE of 2.3 ± 0.1 at basic pH and the pH−SIE profile characterized by a unique pK_a of 7.7 ± 0.1 confirm that the rate-limiting step is associated with deacylation. Moreover, the similarity between this pK_a and the pK_a value of 7.6 obtained in the acylation profile strongly suggests the assignment of this ionization to the same residue, namely, Glu-268. The SIE of 2.3 ± 0.1 observed at basic pH would indicate that the glutamate form of Glu-268 acts as a base catalyst at high pH. Use of the proton inventory method for wild-type GAPN at pH 8.5 showed that the dependence of k_{ss} upon the D_2O mole fraction is essentially linear. Providing that we can exclude such cases when two successive processes within deacylation contribute to the rate, and when the rate is limited by an isotopically sensitive conformational step, both of which can give rise to linear dependencies (*9*), the above result supports that the SIE originates from the transfer of one proton in the rate-limiting transition state. Therefore, at a basic pH, deacylation would be catalyzed by the chemical activation of the water molecule attacking the thioacyl intermediate, via abstraction of one proton by Glu-268. This process would thus be associated with the rate-limiting step within deacylation. For the GAPN-catalyzed reaction, the proton inventory result suggests that catalysis by a coupled multiproton-transfer mechanism, which would involve another residue from the active site, is not likely.

Another essential, although surprising, observation was the relatively high activity of wild-type GAPN in the acidic side of the pH range tested. Indeed, the pH-dependence profiles of k_{ss} and k_{ac} are characterized by two pK_a values of 6.1 and 7.4, indicating the existence of an active "intermediate" species with characteristic rate constant of k_{ss}^{i} of 23 s^{-1}, aside from the basic species characterized by a k_{ss}^{max} of 68 s^{-1}. At pH 6.5, where GAPN likely exists primarily as the intermediate species with Glu-268 under the acidic form, the deuterium solvent isotope effect of 1.1 indicates that the rate-limiting process is no longer associated with proton transfer. Therefore, we propose that, at this pH, Glu-268 catalyzes deacylation through activation and orientation of the attacking water molecule in the active site. Study of the E268A mutant shows a SIE of 4.1 at optimum pH, and a proton inventory curve that bulges downward. This effect could arise from a very large number of protons (the medium effect), in which case the ratio $k_{ss}^{x}/k_{ss}^{D_2O}$ follows an equation of the form Z^x, Z being a constant (*9*). Given the nonlinearity of the log ($k_{ss}^{x}/k_{ss}^{D_2O}$) vs x plot, this hypothesis was not retained (plot not shown). In contrast, this behavior is consistent with two or three protons being transferred in the rate-limiting process. As mentioned in the Results section, analysis of our proton inventory data did not allow further mechanistic deductions. Nevertheless, replacement of Glu-268 by a smaller residue Ala would permit occupation of the site by two or three water molecules. The observed proton transfers between these molecules would not provide efficient catalysis of the hydrolysis process, due to poor activation and/or orientation of these water molecules [compare the rate constants of nonactivated deacylation of *Bacillus stearothermophilus* phosphorylating GAPDH at 25 °C, (*15*), 0.014 s^{-1}, with the optimum rate constant of E268A mutant deacylation, 0.08 s^{-1}]. On the contrary, the presence of a polar side chain such as the one of glutamic acid or glutamine residues would restrict the site to one water molecule and would potentially provide H-bond acceptors to activate and orient this molecule. Indeed, a k_{ss} constant of 0.8 s^{-1} is observed for the E268Q mutant, attesting to significant activation of the rate-limiting deacylation step (unpublished results). Comparison of the difference in the characteristic rate of deacylation between the basic and the intermediate species, which would correspond to Glu-268 protonation in our interpretation (factor of 3 at 0.2 mM D-G3P), and of the effect of substitution of Glu-268 by Ala at basic pH (factor of 850), suggests that, in the GAPN proteic context of the active site, activation and orientation of the attacking water molecule is the major role of Glu-268. In the deacylation, deprotonation of Glu-268 would result in substitution of an already efficient intermediate form with k_{ss}^{i} = 23 s^{-1} (with Glu-268 as carboxylic acid) by a basic form (carboxylate) whose base catalyst capacity only results in a ~3-fold activation of the deacylation rate (k_{ss}^{max} = 68 s^{-1}, see Figure 3) under our experimental conditions.

Various hypotheses can be raised regarding the assignment of the 6.1 pK_a: it could correspond to the side chain of an amino acid residue, to enzyme intermediate groups (C-1 hydroxyl or phosphate), or to NADP phosphate ionizations. Similar arguments as those developed in the preceding section suggest that this pK_a does not reflect the ionization of the phosphate groups of the substrate or cofactor. Moreover, the rate-determining step within deacylation has been associated with the hydrolysis from the solvent isotopic effect. If the observed deacylation rate does not include any contribution from preceding steps of the acylation, and as already suggested for Cys proteases (*20*), assuming that the mechanistic path of deacylation includes a tetrahedral intermediate whose breakdown is not rate-limiting, then the pK_a of 6.1 would not originate from Cys-302 free thiolate but would rather reflect the ionization of the hydroxyl group of this intermediate.

Catalytic Mechanism of GAPN in Relation to Other ALDHs. These results and their interpretations leave several questions unanswered. First, in contrast to published data (*3*, *4*), we show that mutation of Glu-268 does not modify the nature of the limiting step, which remains deacylation. It is a priori not obvious how to reconcile these contradictory results. First, we have demonstrated that the binding of D-G3P to the apo-like binary complex E268A GAPN−NADP induces the formation of a competent ternary complex (*5*). On the other hand, for human liver mitochondrial ALDH, the rate-limiting step of two other mutants was shown to depend on the chemical structure of the substrate (*16*). This leads us to speculate that the formation of a ternary complex competent for acylation can depend on the nature of the substrate. Second, the nature of the molecular and structural factors involved in decreasing the Cys-302 pK_a, in facilitating the hydride transfer, and in stabilizing the thioacyl intermediate remains to be determined. Inspection of the modeled ternary complex of mitochondrial ALDH (*14*), although it might not represent exactly the active structure, suggests that the invariant Asn-169 could be involved. The combined observations of a substrate isotopic effect on the acylation rate and of the very low efficiency of the acylation step for the N169A or N169T mutants have already confirmed the critical role of this residue in the GAPN-catalyzed acylation reaction in forming an oxyanion hole and in facilitating the hydride transfer (unpublished results).

The minimal scenario of the catalytic mechanism of GAPN, a member of the ALDH family close to the class 2 mammalian enzymes, could be hypothesized as follows (Figure 6). First, the binding of NADP to GAPN induces a local conformational rearrangement of the nicotinamide subsite with at least reorientation of both lateral chains of Cys-302 and Glu-268 and repositioning of the nicotinamide ring of NADP. This local reorganization renders Cys-302 more accessible, leads to pK_a shifts of Cys-302 and Glu-268 from 8.5 to 6.2 and from 4.6 to 7.5, respectively, and brings the side chains of Cys-302 and Glu-268 to an interacting distance less than 4 Å (*5*). In this holo complex, amide peptide nitrogens of residues 302 and 303 (*14*), the positive charge of the nicotinamide ring of NADP (*5*), and possibly other structural elements would stabilize the thiolate form of Cys-302 (*14*). Binding of D-G3P then leads to the formation of a thiohemiacetal intermediate in which the hydroxyl group might be stabilized in an oxyanion hole, possibly involving Asn-169. The pK_a of this hydroxyl group would be decreased such that it is deprotonated, thus permitting hydride transfer without base-catalyst assistance. In the next step, which consists of the nucleophilic attack of a water molecule on the thioacyl intermediate, the tetrahedral intermediate could be stabilized by an oxyanion hole including Asn-169, while the principal role of Glu-268 would be to activate and to orient the water molecule, and in addition, to act as a base catalyst at basic pH values.

From an evolution point of view, it is interesting to compare the chemical mechanism of GAPN and of phosphorylating GAPDH, although they belong to structurally unrelated families (*18*, *19*). Both enzymes share the same substrate and the same thioacyl intermediate, which is subsequently either hydrolyzed or phosphorylated. Clearly, in these two families, different routes have evolved to achieve efficient catalysis of the acylation step. In GAPDHs from bacteria or eucarya, a His residue was shown to participate in decreasing the apparent pK_a of essential Cys-149 via an ion-pair interaction, to act as a base catalyst in the activation of the hydride transfer, and presumably to be involved in the stabilization of the covalent intermediates (*17*). As shown in this work, the picture is totally different in GAPN, where no His residue is involved.

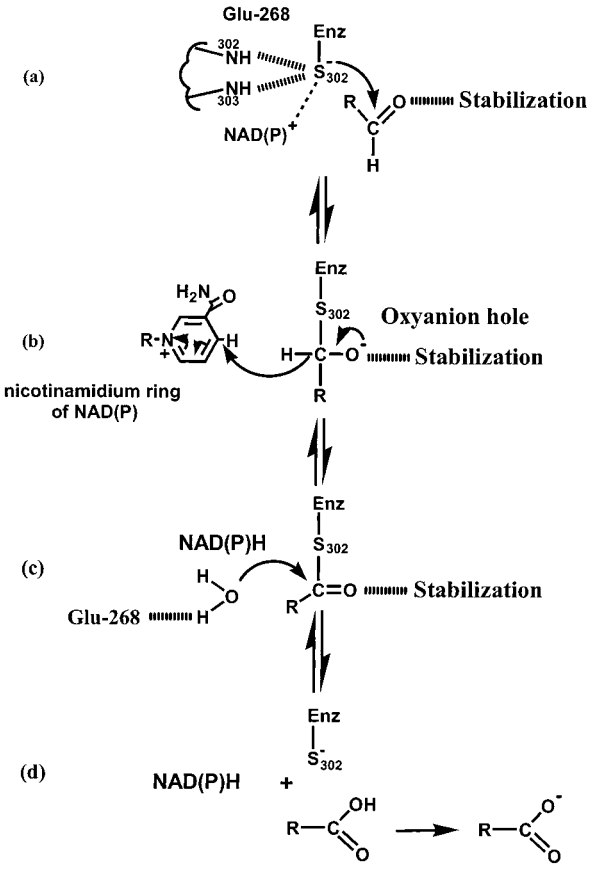

FIGURE 6: Minimal scenario for GAPN catalysis. (a) In holo-GAPN, amide peptide nitrogens of residues 302 and 303 (*14*), the positive charge of the nicotinamidium ring of NADP (*5*), and possibly other structural elements stabilize the thiolate form of Cys-302. (b) Stabilization of the thiohemiacetal intermediate as an oxyanion, possibly involving Asn-169 side chain. (c) Activation of the deacylation by Glu-268, mainly through stabilization and orientation of the water molecule, and general base catalysis at a basic pH. (d) Release of product and reduced cofactor.

ACKNOWLEDGMENT

We are grateful to Dr. M. Hebrant for his technical assistance with the stopped-flow experiments. We thank the Service Commun de Biophysicochimie of University Henri Poincaré, Nancy I, for giving us the possibility to carry out molecular modeling and to E. Habermacher, S. Boutserin, and S. Azza for their very efficient technical help.

REFERENCES

1. Farres, J., Wang, T. T., Cunningham, S. J., and Weiner, H. (1995) *Biochemistry 34*, 2592−2598.
2. Vedadi, M., Szittner, R., Smillie, L., and Meighen, E. (1995) *Biochemistry 34*, 16725−16732.
3. Wang, X., and Weiner, H. (1995) *Biochemistry 34*, 237−243.
4. Vedadi, M., and Meighen, E. (1997) *Eur. J. Biochem. 246*, 698−704.

5. Marchal, S., and Branlant, G. (1999) *Biochemistry 38*, 12950−12958.
6. Segel, I. H. (1968) in *Enzyme kinetics. Behavior and analysis of rapid equilibrium and steady-state enzyme system*, 3rd ed., John Wiley & Sons, Inc.
7. Pinitgland, S., Watts, A. B., Patel, M., Reid, J. D., Noble, M. A., Gul, S., Bokth, A., Naeem, A., Patel, H., Thomas, E. W., Sreedharan, S. K., Verma, C., and Brocklehurst, K. (1997) *Biochemistry 36*, 9968−9982.
8. Salomaa, P., Shaleger, L. L., and Long, F. A. (1964) *J. Am. Chem. Soc. 86*, 1−8.
9. Cook, P. F., Ed. (1994) *Enzyme Mechanisms from Isotope Effects*, CRC Press, Boca Raton, FL.
10. Cobessi, D., Tete-Favier, F., Marchal, S., Azza, S., Branlant, G., and Aubry, A. (1999) *J. Mol. Biol. 290*, 161−173.
11. Dawson, R. A. C., Elliot, D. C., Elliot, W. H., and Jones, K. M. (1979) *Data for Biochemical Research*, 2nd ed., Clarendon Press, Oxford, England.
12. Cleland, W. W. (1982) *Methods Enzymol. 87*, 390−405.
13. Eyschen, J., Vitoux, B., Rahuel-Clermont, S., Marraud, M., Branlant, G., and Cung, M. T. (1996) *Biochemistry 35*, 6064−6072.
14. Steinmetz, C. G., Xie, P., Weiner, H., and Hurley, T. D. (1997) *Structure 5*, 701−711.
15. Michels, S., Rogalska, E., and Branlant, G. (1996) *Eur. J. Biochem. 235*, 641−647.
16. Ni, L., Sheikh, S., and Weiner, H. (1997) *J. Biol. Chem. 272*, 18823−18826.
17. Talfournier, F., Colloc'h, N., Mornon, J. P., and Branlant, G. (1998) *Eur. J. Biochem. 252*, 447−457.
18. Skarzynski, T., and Wonacott, A. J. (1988) *J. Mol. Biol. 203*, 1097−1118.
19. Duée, E., Olivier-Deyris, L., Fanchon, E., Corbier, C., Branlant, G., and Dideberg, O. (1996) *J. Mol. Biol. 257*, 814−838.
20. Szawelski, R. J., and Wharton C. W. (1981) *Biochem. J. 199*, 681−692.

BI9914208